Zonal wave structures in the nighttime tropospheric density and temperature and in the *D* region ionosphere over Mars: Modeling and observations

S. A. Haider,[1,2] M. A. Abdu,[1] I. S. Batista,[1] J. H. A. Sobral,[1] Varun Sheel,[2] G. J. Molina-Cuberos,[3] W. C. Maguire,[4] and M. I. Verigin[5]

Received 11 March 2009; revised 23 July 2009; accepted 20 August 2009; published 22 December 2009.

[1] We report the first model results of zonal wind perturbations in the nighttime *D* region ionosphere of Mars during winter and summer seasons at latitude ranges 60°S–64°S and 64.7°N–67.3°N, respectively. The production rate, ion density, and electron density are calculated between longitudes 0° and 360°E due to impact of galactic cosmic rays on the nighttime troposphere of Mars at these latitudes. In this calculation, temperature and air density are used from the measurements made by the radio occultation experiment on board Mars Global Surveyor at low solar activity period. In these seasons the zonal distribution of temperature, air density, and electron density are fitted by a least squares method at altitudes near the surface, 15 km and 30 km. The modes of seasonal winds are also calculated from Fourier analysis at these heights. These measurements suggest mode of wave number 2 in northern high latitudes and wave numbers 3 and 8 in southern high latitudes, respectively. It is found that the nighttime ionosphere of Mars consists of a permanent *D* peak, which varies with east longitudes in both hemispheres. The modes 2 and 3 of semidiurnal tides dominate the *D* peak oscillation during the summer and winter seasons, respectively. The water cluster ions $H_3O^+(H_2O)_n$, $NO_2^-(H_2O)_n$ and $CO_3^-(H_2O)_n$ are the major species in the *D* region ionosphere of Mars.

Citation: Haider, S. A., M. A. Abdu, I. S. Batista, J. H. A. Sobral, V. Sheel, G. J. Molina-Cuberos, W. C. Maguire, and M. I. Verigin (2009), Zonal wave structures in the nighttime tropospheric density and temperature and in the *D* region ionosphere over Mars: Modeling and observations, *J. Geophys. Res.*, *114*, A12315, doi:10.1029/2009JA014231.

1. Introduction

[2] Mars has the highest orbital eccentricity of any planet except Mercury. The distance from the Sun to Mars varies from 1.64 AU to 1.36 AU over a Martian year. This large variation, combined with an axial tilt gives rise to seasonal changes far greater than what we experience on Earth. Since a year on Mars lasts twice as long as a year on Earth, the Martian seasons are twice as long as well. The big change in distance during the orbit causes the two hemispheres to receive different amounts of sunlight during their summers and winters. Mars is closest to the Sun during the southern summer and northern winter. The summer temperature in the south can be ~30°C warmer than the equivalent summers in north. The changing seasons and temperature differences across the planet produce huge dust storms [*Martin*, 1984]. Some storms can affect just a small area, while others can cover the entire planet. They usually happen when the planet is nearing its closest point to the Sun.

[3] Theories of photochemistry, ion chemistry, and dayglow of Mars are now well developed and tested for specific times and locations of spacecraft observations [*Barth et al.*, 1992]. Thermal structure is also reasonably well understood, although some of the parameters have been determined empirically. The challenge for the future is to observe diurnal and seasonal changes that occur over the entire Martian globe. The solar energy input varies with different periods such as daily rotation of Mars, season of Mars, 27 day rotation period of the Sun, 11 year cycle of the solar activity and episodic events associated with solar flares. Such observations under changing conditions will be important on Mars in the future.

[4] Mars Global Surveyor (MGS) has observed temperature, density and pressure from a radio occultation experiment for over 3 Martian years in the northern and southern hemispheres. This experiment has been found very useful for Mars' ionosphere/atmosphere observations. In this experiment S and X band radio waves were used simultaneously to determine the frequency dependence of the phase and amplitude variations [*Hinson et al.*, 1999]. The S band frequency of 2.3 GHz was used to measure the plasma

[1]Instituto Nacional de Pesquisas Espaciais, São José dos Campos, Brazil.
[2]Physical Research Laboratory, Ahmedabad, India.
[3]Universidad de Murcia, Murcia, Spain.
[4]NASA Goddard Space Flight Center, Greenbelt, Maryland, USA.
[5]Space Research Institute, Moscow, Russia.

Copyright 2009 by the American Geophysical Union.
0148-0227/09/2009JA014231

density of Mars and the X band frequency of 8.4 GHz was used to measure the neutral density, temperature and pressure of Mars. These measurements are made available by the radio science team at NASA's Planetary Data System (http://pds-geosciences.wustl.edu/missions/mgs/radioscience.html).

[5] In this paper we have used temperature and air density profiles measured by the radio occultation experiment in the northern and southern hemispheres at nighttime. The data sets for the northern hemisphere are composed of 36 profiles of temperature and density. These observations were made after midnight (at local time 0300–0400 h) on 24–31 December 1998 near solar longitude (Ls) = 74°–77° at latitudes 64.7°N–67.3°N and solar zenith angle 78°–81°. The data sets for the southern hemisphere were obtained in the late evening (after sunset at local time 2200–0100 h) from 23 profiles of temperature and density, which were observed on 2–15 March 1998 near Ls = 285°–291° at latitudes 60°S–64°S and solar zenith angles 90°–93°. Both observations are carried out in troposphere at different longitudes between 0 and 360°E. At the time of these measurements Mars had winter in south and summer in north with moderate solar activity period ($F_{10.7}$ = 132–181).

[6] The lower atmosphere of Mars consists of troposphere and isothermal mesosphere at altitudes between 0 to 40 km and 40 to 90 km, respectively [*Mahajan and Kar*, 1988]. The *D* layer is formed in the troposphere at altitude range ~25–35 km [*Haider et al.*, 2009]. The first theoretical study of the lower ionosphere of Mars was reported by *Whitten et al.* [1971]. They calculated the electron density in the dayside ionosphere of Mars due to ionization by cosmic rays and solar radiation. *Molina-Cuberos et al.* [2002] have also used these sources of ionization to obtain the electron density profiles for the Martian dayside ionosphere. Later *Haider et al.* [2007, 2009] have modeled the electron density in *D*, *E*, and *F* regions due to absorption of solar EUV, solar wind electron and galactic cosmic rays in the daytime/nighttime Martian ionosphere. Recently, we have developed a model to calculate the production rate and densities in the troposphere of Mars. Using this model the densities of ions and electrons were estimated in the summer and winter seasons at high latitude [*Haider et al.*, 2008]. This model is extended now to study the zonal wave oscillations in the nighttime Martian troposphere at nearly same latitude and same solar zenith angle. The ion production rates are calculated at high solar zenith angles between longitudes 0 and 360°E due to impact of galactic cosmic rays with the gases of northern and southern troposphere of Mars. The production rate and temperature have been used later in the continuity equation for the calculations of ion and electron densities under steady state condition.

2. Objective

[7] The objective of this paper is to study the dynamical perturbations in the nighttime troposphere of Mars. We have calculated the longitudinal distribution of production rates, ion and electron densities due to impact of galactic cosmic rays with the gases of the Martian troposphere at high northern and southern latitudes during summer and winter seasons, respectively. The oscillations related to long planetary-scale waves and baroclinic instability processes have been studied in the upper atmosphere of Mars [*Seth et al.*, 2006; *Seth and Brahmananda Rao*, 2008]. This study is not carried out in the nighttime *D* region ionosphere of Mars due to insufficient observations. Mars is a very windy planet. Various types of atmospheric motions are expected to exist in the troposphere of Mars. The wind is composed of gravity waves, tidal waves and stationary waves. At high altitudes (~100–120 km) the gravity waves dissipate rapidly due to molecular viscosity and thermal conduction because of their short wavelengths [*Imamura and Ogawa*, 1995]. Larger-scale winds such as tidal oscillations are thought to be the dominant modes of the motion in the thermosphere of Mars [*Bougher et al.*, 2001]. *Cavalie et al.* [2008] have reported that zonal winds are representative of the Martian seasons. One needs to know what mode of the zonal wind predominates in the troposphere of Mars. The propagating winds can lead to variations in the nighttime tropospheric temperature and density. In this paper we report wave like longitudinal variations of temperature and density in northern and southern troposphere of Mars. Modeling of waves induced ionosphere motion is also carried out in both hemispheres. The propagation of 2 and 3 modes of the semidiurnal atmospheric tide are found to be the dominant cause of the troughs and sinks in the longitudinal distribution profiles of peak electron density and peak altitude. The ion production rate is directly proportional to the neutral density. Therefore, the local maxima and minima of neutral densities at fixed height will translate into corresponding electron density peaks and troughs. A weak variation in electron density as a function of temperature (altitude and longitude dependence) can also exist owing to its influence upon ions.

3. Modeling and Analysis of Data

3.1. Analytical Spectral Fitting

[8] The characteristic of longitudinal distribution of temperature and density in the Martian troposphere is assumed to be approximated as follows:

$$Z = C_0 + C_1 \sin\psi + C_2 \cos\psi + \ldots C_n \sin(n\psi) + C_n \cos(n\psi) \quad (1)$$

where ψ is east longitude and Z is a function of ψ. The parameters C_0, C_1, $C_2 \ldots C_n$ are calculated using this equation in the matrix form Z = A C, where A is coefficient matrix and C is column matrix of parameters C_1 to C_n. This approach is similar to the approximation used by *Bougher et al.* [2001] and *Mahajan et al.* [2007] for studying longitudinal variations in the thermosphere/ionosphere of Mars. We have employed the above equation for a least squares spectral fitting in the calculations based on observational data to characterize the zonal structures in the Martian troposphere. This model contains a constant temperature or density term, an amplitude and phase for a sinusoid with one cycle per 360° of the longitude which is labeled as wave 1 harmonic and higher harmonics up to and including wave 3 and so on. For waves 2 and 3 it will have 5 and 7 parameters, respectively, which are different for each curve. Figures 1a–1c and 2a–2c represent the nighttime zonal distribution of observed temperatures for altitudes near the surface, 15 km and 30 km during summer and winter seasons at latitudes 64.7°N–67.3°N and 60°S–64°S, respectively. The solid lines are plotted for model fit values to the temperature. The dotted

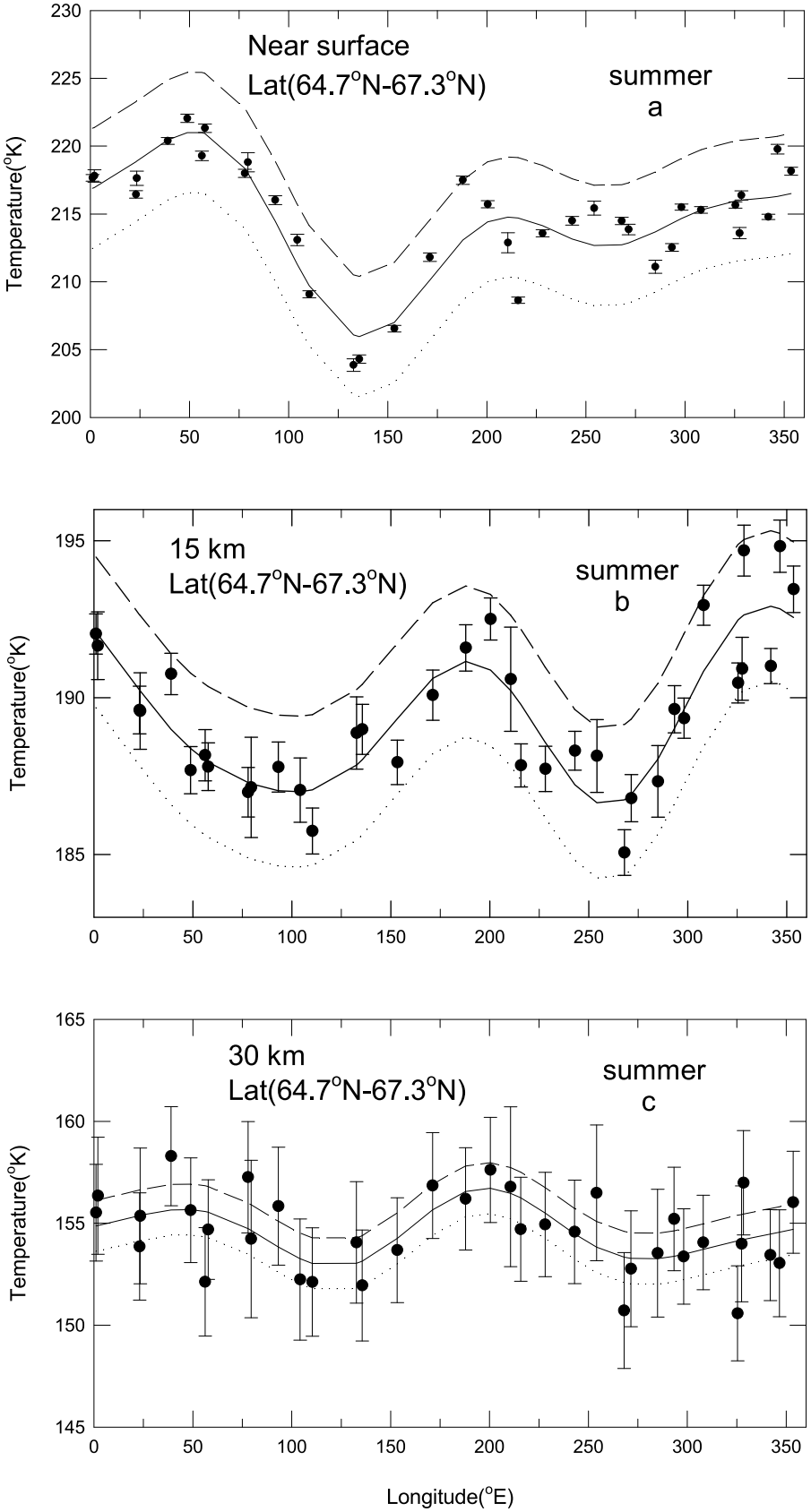

Figure 1. Zonal structures of summer temperature measured by MGS between longitudes 0° and 360°E and latitudes 64.7°N and 67.3°N at altitudes (a) near the surface, (b) 15 km, and (c) 30 km. The solid line represents the best fit to the data. The dotted and dashed lines represent lower and upper 0.95 confidence limits. The error bar is also plotted.

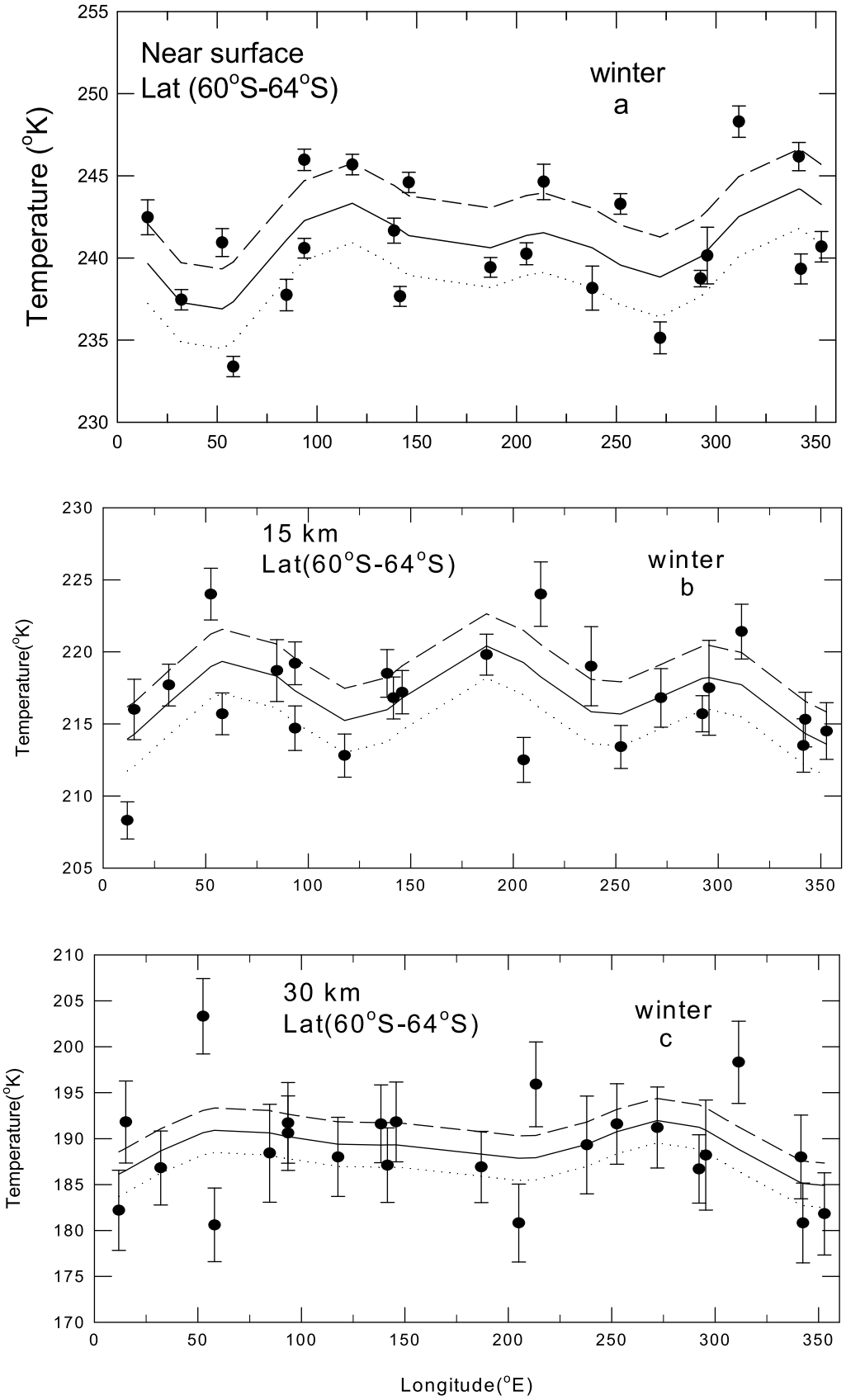

Figure 2. Zonal structures of winter temperature measured by MGS between longitudes 0° and 360°E and latitudes 60°S and 64°S at altitudes (a) near the surface, (b) 15 km, and (c) 30 km. The solid line represents the best fit to the data. The dotted and dashed lines represent lower and upper 0.95 confidence limits. The error bar is also plotted.

and dashed lines are for lower and upper 0.95 confidence limits, respectively. The measurement uncertainties are also shown in Figures 1 and 2, which is much smaller near the surface. However, it increases with altitude. The zonal structure with the significant peaks in the temperatures at ~50°E and ~200°E can be seen in northern summer at altitudes near the surface and 30 km. However, there is a longitudinal delay of ~30° in the second peak of the northern temperature profile at altitude 15 km. Therefore, the first peak is probably absent in the temperature near 50°E at 15 km. The tropospheric temperatures in southern winter do not represent zonal structure clearly in the observed data at 30 km. However, three significant peaks in longitudinal distribution of southern temperature can be seen near 50°E, 200°E and 300°E at 15 km.

[9] Figures 3a–3c and 4a–4c represent the nighttime zonal distribution of the observed density at the same altitudes and latitudes as in Figures 1a–1c and 2a–2c, respectively. The solid lines are plotted using model fit values to the density. The dotted and dashed lines are for lower and upper 0.95 confidence limits, respectively. The measurement uncertainties are also shown in Figures 3 and 4, which is much smaller than in the other observations made by the radio occultation experiment shown in Figures 1a–1c and 2a–2c. The zonal structure with two significant peaks in the density at ~150°E–175°E and ~325°E can be seen in the northern troposphere during the summer season. We have observed three prominent zonal peaks in the density of southern troposphere at ~50°E, 180°E, and 300°E during winter season.

3.2. Fourier Analysis

[10] In the troposphere the wind motion is related to latitude and longitude variations of the temperature profile. The wind speed can be computed approximately from temperature data by using the hydrostatic equation as

$$\frac{\partial p}{\partial y} = p\frac{h}{HT}\frac{\partial T}{\partial y} \tag{2}$$

where h is height, H is scale height, p is pressure and T is the temperature (assumed here not to vary with height). The pressure gradient occurs in the north-south y direction due to the variation of solar heating with latitude and it results in an east-west wind. The pressure gradient is balanced by the Coriolis force $\rho U_x f$ associated with an east-west wind U_x, where f is the standard Coriolis parameter $f = 2\Delta\sin\theta$. Here θ is the latitude and Δ is the angular velocity of Mars. The Martian year is roughly twice as long as the Earth's year. This means that Mars angular speed is half that of Earth. The angular speed of Earth is 7.29×10^{-5} radian/s. Thus,

$$U_x = -\frac{p}{\rho f}\frac{h}{HT}\frac{\partial T}{\partial y} = \frac{-hg}{fT}\frac{\partial T}{\partial y} \tag{3}$$

where ρ is air density and g is Mars' gravitational acceleration equal to 3.72 m/s^2. Using this equation the speed of the wind in summer can be approximately estimated for Figure 1c as ~31 m/s at 30 km altitude with temperature variation $\partial T \approx 6$°K and wind propagating distance $\partial y \approx 2500$ km in about 3 h covering east longitude ~50°E.

[11] The semidiurnal tide has a period of 12 h and covers the Mars circumference ($2\pi R_m$) ~ 21290 km in 24 h, where R_m is the radius of Mars. The various modes of tidal waves can be described by Fourier analysis from the formula given below:

$$a_n = \frac{1}{L}\int_0^L I(x)\cos\left[\frac{2\pi nx}{L}\right]dx \approx \frac{1}{72}\sum_{j=1}^{72} I(x)\cos\left[\frac{2\pi nj}{72}\right] \tag{4}$$

$$b_n = \frac{1}{L}\int_0^L I(x)\sin\left[\frac{2\pi nx}{L}\right]dx \approx \frac{1}{72}\sum_{j=1}^{72} I(x)\sin\left[\frac{2\pi nj}{72}\right] \tag{5}$$

$$I = A_n\sin(K_x + \delta) \tag{6}$$

$$A_n = \text{sqrt}\,(a_n^2 + b_n^2);\ \tan\delta = (b_n/a_n) \tag{7}$$

where K_x is a wave number, a_n and b_n are the amplitudes of the harmonic components of temperature or density I(x) evaluated at 72 equally spaced interval at 5° between longitude 0° and 360°E. These measurements are distributed fairly well between longitude 0° and 360°E. A linear interpolation method is used wherever radio occultation data is not available at these intervals. It has been shown by *Whittaker and Robinson* [1967] that the values of a_n and b_n as obtained above are also the least squares fit of the harmonics. We can also calculate the contribution of each harmonic from the total variance. If D is the zonal distribution of the tropospheric temperature/density then $D = D_m + D_d$, where D_m is the zonal mean and D_d is the deviation. The variance V is given as $V = D^2$. The contribution of each harmonic is $A_n^2/2$. Thus the percentage variance explained by harmonic n is $[A_n^2/2V]$.

[12] In Figures 5 and 6 the normalized amplitudes of different wave numbers for temperature and density of the nighttime are represented, respectively. We compare our calculated Fourier spectrum at altitudes near the surface (Figures 5a and 6a), at 15 km (Figures 5b and 6b), and at 30 km (Figures 5c and 6c) for northern summer and southern winter seasons at nearly same latitudes. Fourier analysis suggests that the temperature and density of nighttime Martian troposphere are dominated by wave number 2 in the northern summer. There are two prominent and distinct peaks at wave numbers around 3 and 8 in the temperature and density profiles of the southern winter. The wave numbers 2 and 3 are associated with semidiurnal oscillations, while the wave number 8 is a class of rapidly moving transient disturbances, which may be associated with baroclinic instability processes. *Seth and Brahmananda Rao* [2008] have found evidence of baroclinic waves in the upper atmosphere of Mars at high latitude. We report that theses waves are initially generated in the troposphere from where they propagate to the upper atmosphere by transport processes. The differences in wave modes between northern and southern hemispheres are due to differences in the topography in these two regions. This is the evidence that tropospheric winds are different in summer and winter

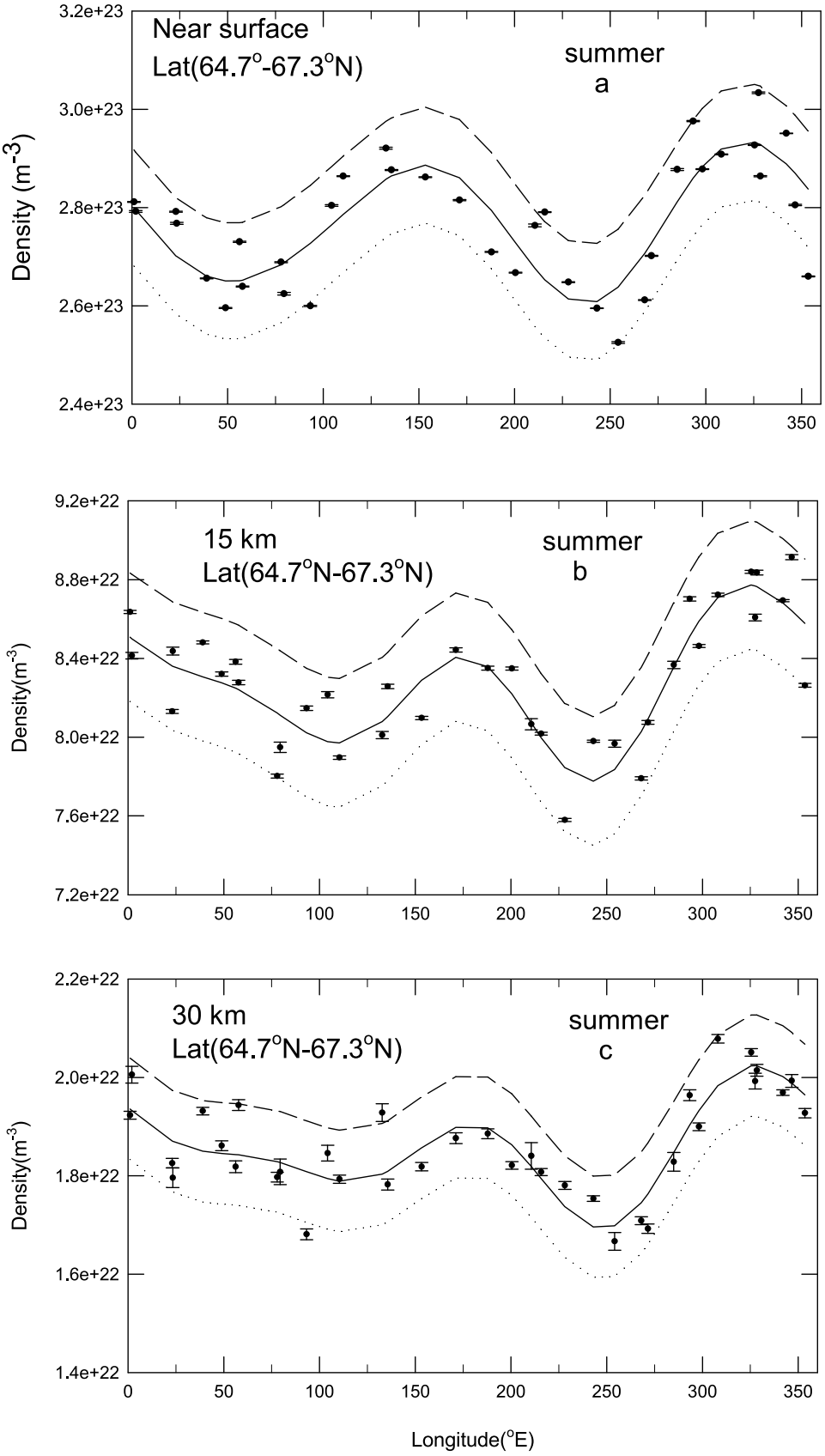

Figure 3. Zonal structures of density measured by MGS during summer between longitudes 0° and 360°E and latitudes 64.7°N and 67.3°N at altitudes (a) near the surface, (b) 15 km, and (c) 30 km. The solid line represents the best fit to the data. The dotted and dashed lines represent lower and upper 0.95 confidence limits. The error bar is also plotted.

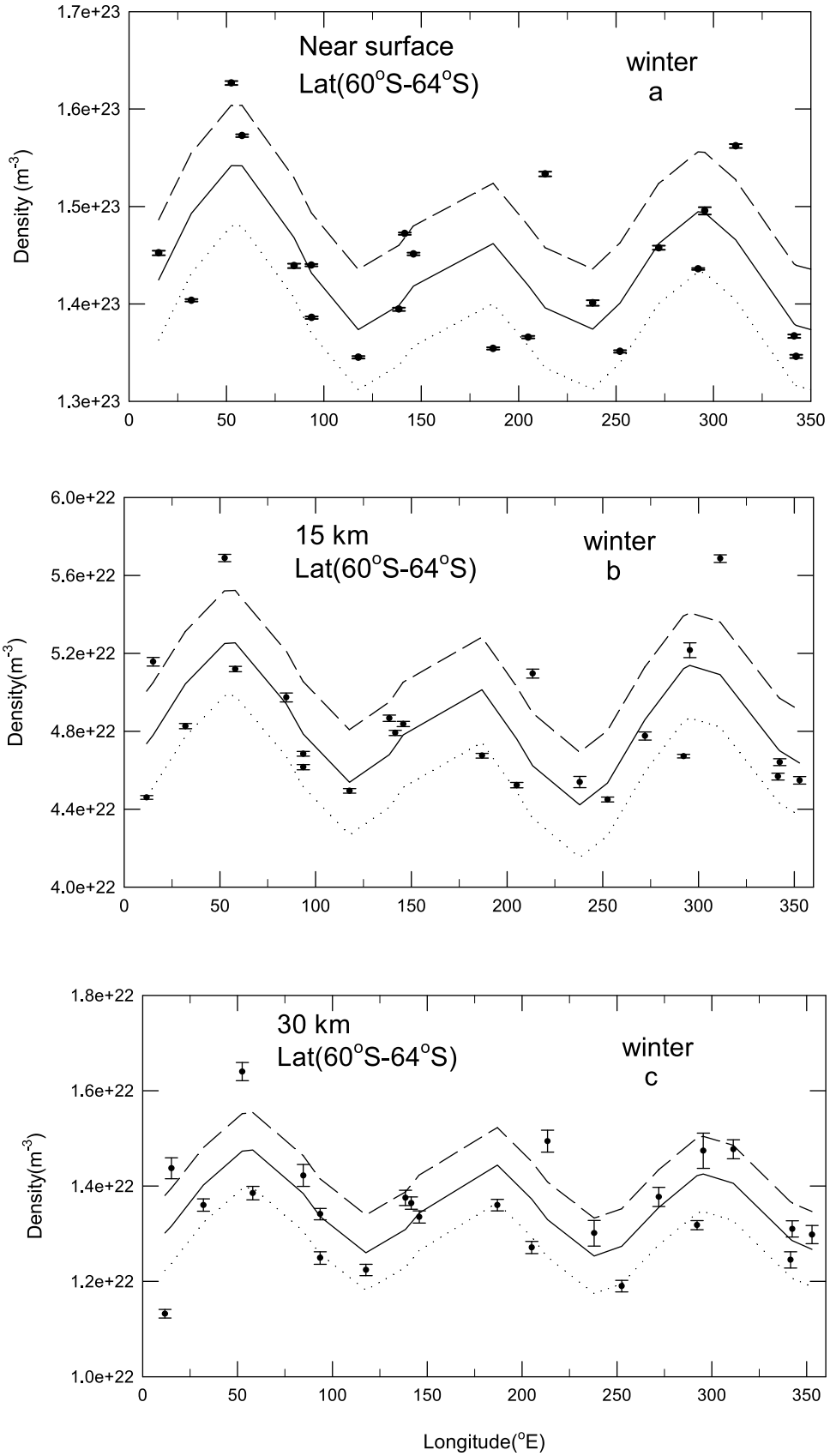

Figure 4. Zonal structures of density measured by MGS during winter between longitudes 0° and 360°E and latitudes 60°S and 64°S at altitudes (a) near the surface, (b) 15 km, and (c) 30 km. The solid line represents the best fit to the data. The dotted and dashed lines represent lower and upper 0.95 confidence limits. The error bar is also plotted.

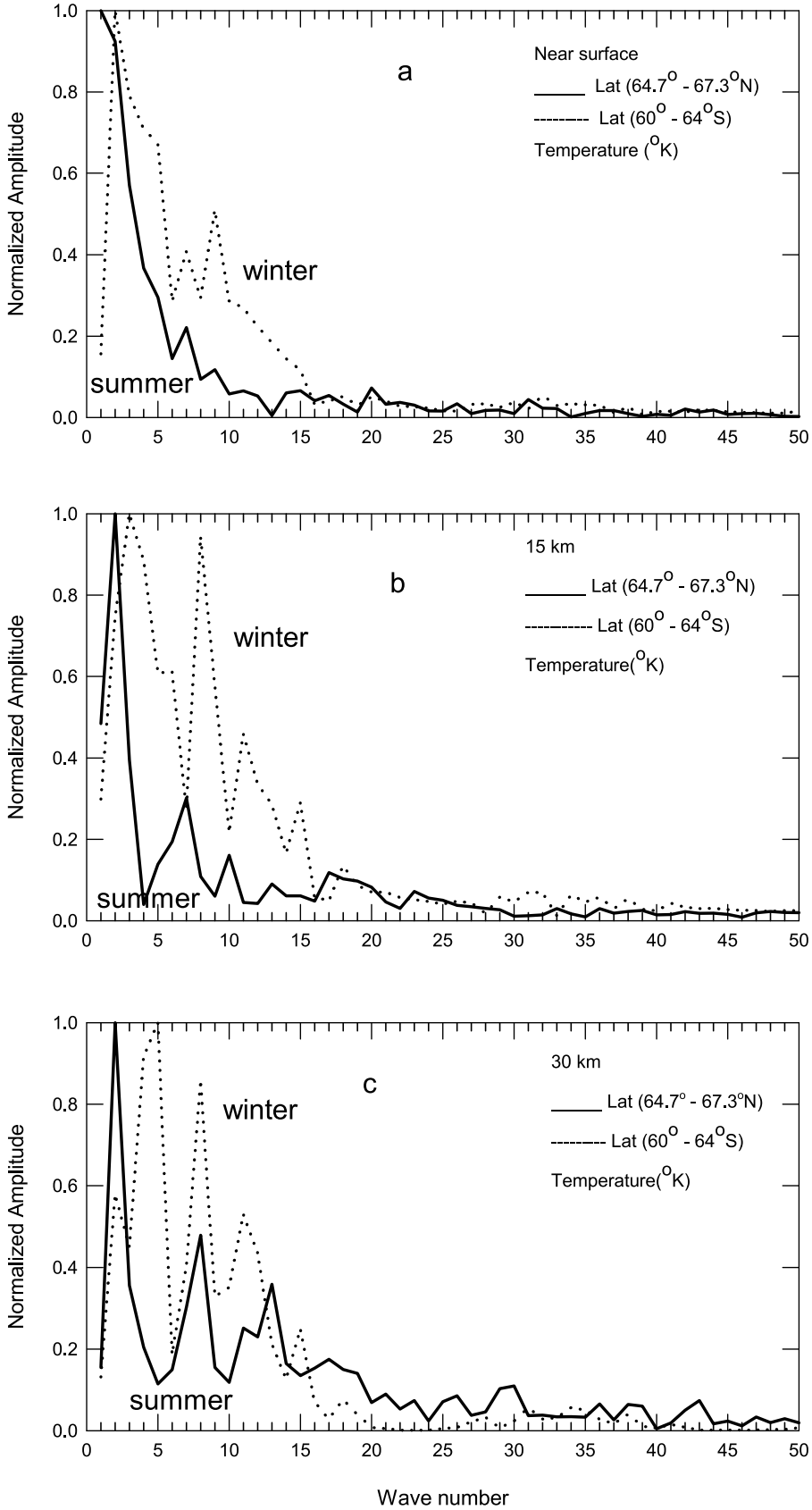

Figure 5. Distribution of normalized amplitude and mode numbers during summer (solid line) and winter seasons (dotted line) due to zonal structures of temperature for latitude ranges 64.7°N–67.3°N and 60°S–64°S at altitudes (a) near the surface, (b) 15 km, and (c) 30 km.

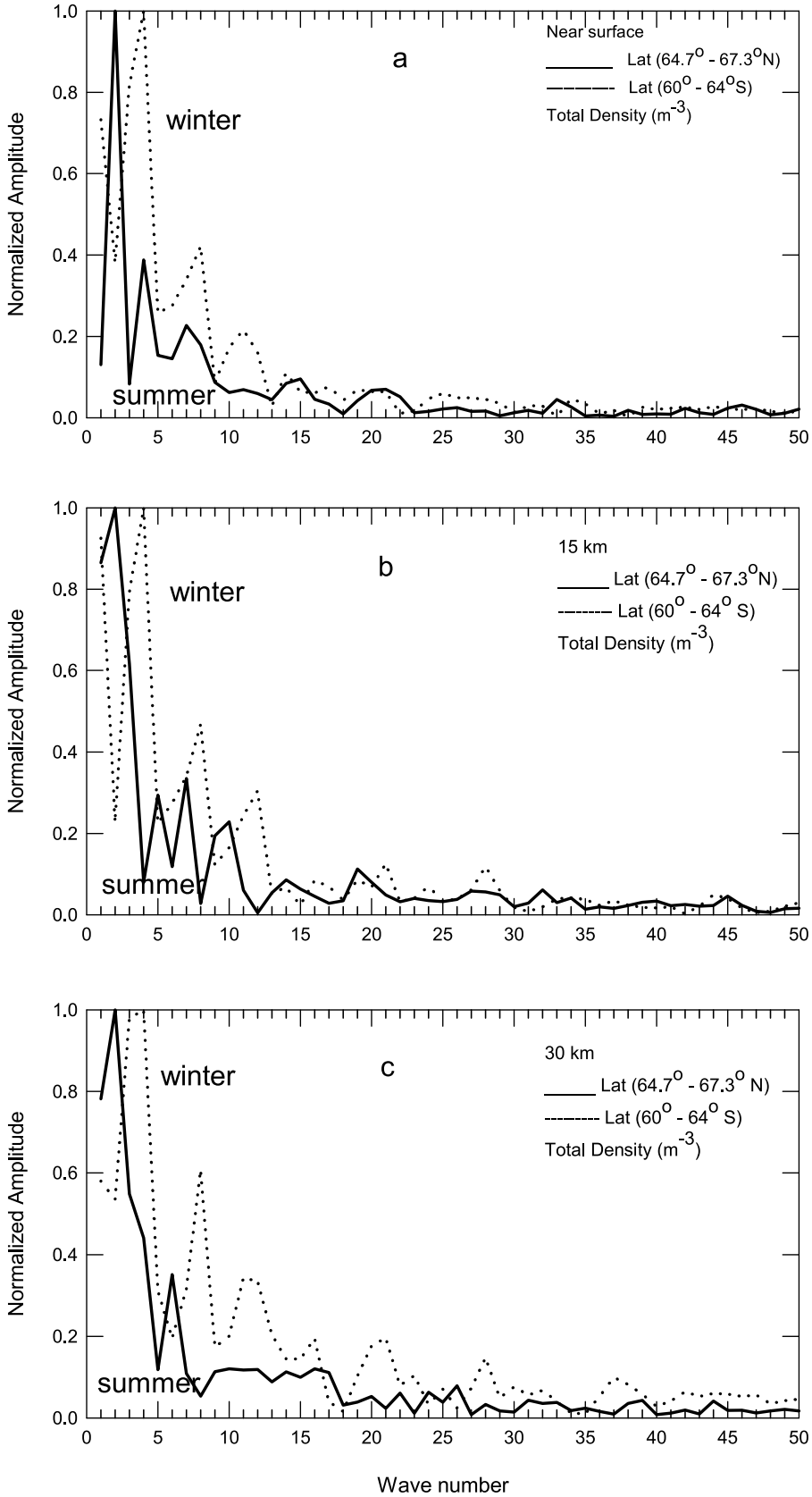

Figure 6. Distribution of normalized amplitude and mode numbers during summer (solid line) and winter seasons (dotted line) due to zonal structures of density for latitude ranges 64.7°N–67.3°N and 60°S–64°S at altitudes (a) near the surface, (b) 15 km, and (c) 30 km.

seasons at high northern and southern latitudes, respectively. The most important difference between the seasons of two different hemispheres is the absence of a second peak in Fourier spectrum at high wave number at northern latitudes.

[13] The Martian troposphere appears to be represented by forced and free oscillations. The forced oscillations are the atmosphere's response to the daily cycle of the Sun, or spatial difference in the heating and topography, while free oscillations include atmospheric instabilities. On Earth the forced oscillations are mainly due to stationary waves, which are induced by topography and ocean-continent heating differences. They have strong control over the weather and thus are important to our daily life. Mars has no ocean. But forced oscillations are important not only through a possible influence on seasons but also by contributing in a significant way to the overall distribution of heat on the planet. The forced oscillations consist of thermal tides and stationary waves. The thermal tides are relatively strong on Mars compared to the Earth [*Banfield et al.*, 2003]. The thermal tides consist not only of the modes that follow the Sun (so-called migrating tides), but also of modes which do not follow the Sun, called nonmigrating tides through the interaction of the winds with topography. The nonmigrating tides are expected to exert their strongest influence in the troposphere, modulating the density. The stationary waves associated with the nonmigrating tides can influence the stability of the atmosphere, enhancing the formation of free disturbances at certain longitudes and impeding their formation at others [*Hollingsworth and Barnes*, 1996].

3.3. Energy Loss Model

[14] In the energy loss model, a charged particle loses its kinetic energy, or is deflected from its original path, involving four principal types of interactions: (1) inelastic collisions with bound atomic electrons whereby a charged particle loses kinetic energy in an absorber (as a result of such collision, one or more atomic electrons experience a transition leading to an excited state or an ionization state of the atom), (2) inelastic collision with a nucleus that causes a deflection of the particle (in some deflections, but not all, a quantum of radiation is emitted (bremsstrahlung), and a corresponding amount of kinetic energy is lost by the colliding particles), (3) inelastic nuclear scattering in which the incident particle is deflected but does not radiate, nor does it excite the nucleus (the incident particle loses the kinetic energy required for conservation of momentum between the two particles), and (4) an incident charge particle may be elastically deflected in the field of the atomic electrons of a struck atom. Energy and momentum are conserved, and the energy transfer is generally less than the lowest excitation potential of the electrons, so that the interaction is really with the atom as a whole. Such collisions are significant for the case of very low energy (<100 eV) incident electrons. In the absorbing material, a moving particle is slowed down and finally brought to rest by the combined action of all four of these elastic and inelastic collision processes. From collision theory, one can obtain the probabilities of any particular type of collision, of any particular energy loss and of any particular change of the direction of motion of incident particle. After the first collision, these probabilities can be applied to a second collision, then to a third etc. The cosmic ray ionization is produced by this method.

[15] The high-energy cosmic rays propagate through the atmosphere, producing nucleonic cascades. The impact of primary cosmic rays, mainly protons and α particle with the atmospheric molecules produces protons, neutrons and pions. Fast secondary nucleons can gain enough energy to increase the production of particles by neutral collisions. Neutral pions quickly decay to gamma rays, and their contribution to the energy deposition is very important in the lower part of the atmosphere. At high altitudes the maximum ion production rates are due to protons. Charged pions decay to muons, which do not decay before reaching the ground and hence the muon energy is transferred to the surface. The production rates due to absorption of galactic cosmic rays at solar zenith angle χ are given below:

$$q(h,\chi) = \frac{1}{Q}\int_E\int_\Omega (dE/dh)F(\chi,E,\Omega)d\Omega dE \tag{8}$$

where Q = 35 eV is the energy required for the formation of an electron ion pair; (dE/dh) is the energy loss due to ionization of the gas, F is the total differential flux and Ω is the spatial angle. The formulae of the total differential flux of galactic cosmic rays and their attenuation loss in the Martian atmosphere have been derived in detail by *Haider et al.* [2008]. The flux of incident galactic cosmic rays is calculated to be between 10^3 to 10^{-5} particles m^{-2} s^{-1} GeV^{-1} sr^{-1} for energy range 1–1000 GeV. We do not know what fraction of galactic cosmic rays actually precipitate at high northern and southern latitudes during summer and winter seasons. Therefore, we have used the same energy flux of galactic cosmic rays in both model calculations. Since the cosmic rays penetrate isotropically into the atmosphere, equation (8) reduces as follows:

$$q(h,\chi) = \frac{2\pi}{Q}\int (dE/dh)\ F(\chi,E)dE. \tag{9}$$

There does not exist any observed model atmosphere, which can give altitude profiles of neutral compositions in the Martian troposphere at different latitudes and longitudes. Modeling has provided a better knowledge of the neutral compositions and structures. *Rodrigo et al.* [1990] and *Nair et al.* [1994] have modeled the atmospheric constituents CO_2, N_2, A_r, O_2, CO, H_2O, H_2, O, O_3, NO, NO_2, and HNO_3. *Molina-Cuberos et al.* [2002] have used this model atmosphere to study the daytime lower ionosphere of Mars. Later *Haider et al.* [2007, 2009] have used this model in the daytime and nighttime ionosphere of Mars. In this paper we have obtained two model atmospheres of these gases between longitudes 0° and 360°E; one model for northern latitudes 64.7°N–67.3°N and the other model for southern latitudes 60°S–64°S from measured air density by multiplying it by the mixing ratios of their gases [*Rodrigo et al.*, 1990; *Nair et al.*, 1994; *Tyler et al.*, 2001]. The same mixing ratios are taken in both model atmospheres. Variation in mixing ratios can vary neutral density of minor constituents. The concentrations of major gases are not much affected because of the change in the mixing ratios. Additional refinement of meteorological models and further calibration

of mass spectrometer data may be expected to change the mixing ratios somewhat in both hemispheres. But it will require additional in situ measurements of the Martian atmosphere to bring about substantial improvements. Each model atmosphere is constructed from the observed density (shown in Figures 3 and 4) at 72 longitudes and 200 heights starting from 0° to 360°E and 1 to 40 km using intervals of 5° and 0.2 km, respectively. To calculate electron density, the temperature is taken from the observations (shown in Figures 1 and 2) at these altitudes and longitudes.

4. Results and Discussion

[16] In Figures 7 and 8, we represent the nighttime zonal distribution of the production rates of CO_2^+ estimated at high northern and southern latitudes, respectively, for altitudes near the surface (Figures 7a and 8a), at 15 km (Figures 7b and 8b), and at 30 km (Figures 7c and 8c). The production rates of other ions (N_2^+, A_r^+, O_2^+, CO^+, H_2O^+, H_2^+, O^+, O_3^+, NO^+, NO_2^+, and HNO_3^+) are lower by 2 to 10 orders of magnitudes, therefore they are not plotted in Figures 7 and 8. We have employed equation (1) for least squares spectral fitting to the calculation to characterize the zonal structures in the Martian troposphere. The variability in the production rates has one-to-one correspondence to the measured neutral density wave structures (see Figures 3 and 4). These production rates are used to calculate the densities of 35 ions, namely, A_r^+, O_2^+, CO_2^+, $O_2^+CO_2$, NO^+, H_3O^+, $H_3O^+H_2O$, $H_3O^+(H_2O)_2$, $H_3O^+(H_2O)_3$, $H_3O^+(H_2O)_4$, H_3O^+HO, $CO_2^+CO_2$, CO^+, C^+, N_2^+, NO^+CO_2, N^+, $O_2^+(CO_2)_2$, $O_2^+H_2O$, $O_2^+(H_2O)_2$, O_4^+, O^+,$CO_3^-H_2O$, $CO_3^-(H_2O)_2$, CO_3^-, CO_4^-, NO_2^-, $NO_2^-H_2O$, $NO_2^-(H_2O)_2$, NO_3^-, $NO_3^-H_2O$, $NO_3^-(H_2O)_2$, O_2^-, O_3^-, and O^- at nighttime. Of the 35 profiles the number density of five major positive ions H_3O^+, $H_3O^+H_2O$, $H_3O^+(H_2O)_2$, $H_3O^+(H_2O)_3$ and $H_3O^+(H_2O)_4$ are shown in Figures 9a and 9b at latitudes 64.7°N and 64°S for summer and winter seasons, respectively. The ion neutral reactions and their rate coefficients are taken from our previous paper [*Haider et al.*, 2007]. We have used 117 chemical reactions, which include ion-neutral and electron-neutral reactions, dissociation of positive and negative ions, electron detachment, ion-ion and ion-electron recombination processes. Three body reactions are very important at Mars, but most of them have been measured using N_2 or O_2 as a third body and the rate coefficient with CO_2 is unknown. When no rate coefficient for CO_2 is available, we have used the known data as valid for Mars' atmosphere conditions. However, the rate coefficient does not depend too much on the third body. It is known that the three body reaction rate coefficient asymptotically approaches a limit at high pressure and that the high-pressure behavior of such reactions is similar to bimolecular processes. The density of the Martian atmosphere is not high enough to saturate the trimolecular reactions included in this model and no limit in the effective bimolecular rate was used here. The transport of molecular ions is not considered in this model calculation because the transport time is several orders of magnitude higher than the chemical life time.

[17] The densities of five major negative ions (CO_4^-, CO_3^-, $CO_3^-H_2O$, $CO_3^-(H_2O)_2$, and $NO_2^-(H_2O)$ are shown in Figures 10a and 10b for the same locations as shown in Figures 9a and 9b. Water cluster of CO_3^- and NO_2^- (i.e., $CO_3^-(H_2O)_n$, $NO_2^-(H_2O)_n$ for n = 1 and 2) are the dominant ions below 30 km. Above this altitude electrons play an important role in the troposphere of Mars. The electron density is plotted in both Figure 10a and Figure 10b. The relative high abundance of oxygen bearing molecules permits the presence of negative ions in the lower ionosphere. Near the surface, the densities of negative ions and electron are reduced by about an order of magnitude in the northern summer than that of the southern winter. This is due to large neutral densities reacting in northern hemisphere by a factor of 2–3 times greater than that of the southern hemisphere [cf. *Haider et al.*, 2008]. The chemistry of the negative ions close to the surface is very sensitive to the neutral density. The position of the ionization peak is also varying between these two seasons. In summer the ionization peaks are found at altitudes ~25 km for ions $CO_3^-H_2O$, CO_3^- and CO_4^- and 28 km for ion $NO_2^-H_2O$. In winter the maximum ionizations for ions CO_3^-/CO_4^- and $NO_2^-H_2O$ occur at altitude ~20 km and 7 km, respectively. The ions $CO_3^-H_2O$ and $CO_3^-(H_2O)_2$ do not represent clear ionization peaks in southern and northern seasons, respectively. In Figures 9a, 9b, 10a, and 10b, the shape and positions of altitude profiles of major positive/negative ions are nearly same with that of our previous calculations [*Haider et al.*, 2008] because the neutral densities, latitudes and longitudes are nearly same between these two calculations. However, the peak electron densities are different in both calculations. In the present calculation the maximum electron densities in winter and summer are obtained as ~80 cm^{-3} and 90 cm^{-3} at altitudes ~26 km and ~30 km, respectively. In Figures 11a and 11b the calculated peak electron densities of 36 and 23 profiles are illustrated for summer and winter seasons, respectively, as a function of longitude. We have used equation (1) for least squares fitting to the calculated peak electron densities to characterize the nighttime zonal structures in the *D* region ionosphere of Mars.

[18] In the *D* region ionosphere, there are significant numbers of positive and negative ions. Under the chemical equilibrium condition electrical neutrality is required as $N_e + N_- = N_+$, where N_e, N_- and N_+ are the concentrations of electrons, negative ions and positive ions, respectively. Since the negative and positive ions may also recombine with each other, the overall balance between production and loss is now expressed as, $q = \alpha_e N_e N_+ + \alpha_i N_- N_+$, where q is production rate, α_e and α_i are the recombination coefficients for the reactions of positive ions with electrons and negative ions, respectively. If the ratio between negative ions and electron concentrations is represented by λ, then in terms of λ, $N_- = \lambda N_e$ and $N_+ = (1 + \lambda)N_e$ and thus $q = (1 + \lambda)(\alpha_e + \lambda\alpha_i)N_e^2$, which becomes as $q = (1 + \lambda)\alpha_e N_e^2$ for $\lambda\alpha_i \ll \alpha_e$. Thus, the equilibrium electron density in the *D* region ionosphere is proportional to the square root of the ion production rate and its magnitude is changed to $q = \alpha_e N_e^2$, when $\lambda \ll 1$, which applies in the upper ionosphere, where negative ions are absent. Therefore, the local maxima and minima of neutral densities at a fixed height will translate into corresponding electron density peaks and troughs. A weak variation in the electron density as a function of temperature (altitude and longitude dependence) also exists owing to its influence upon ions. We have found two prominent zonal peaks in the winter and summer seasons at 110°E and 240°E in the longitudinal distribution

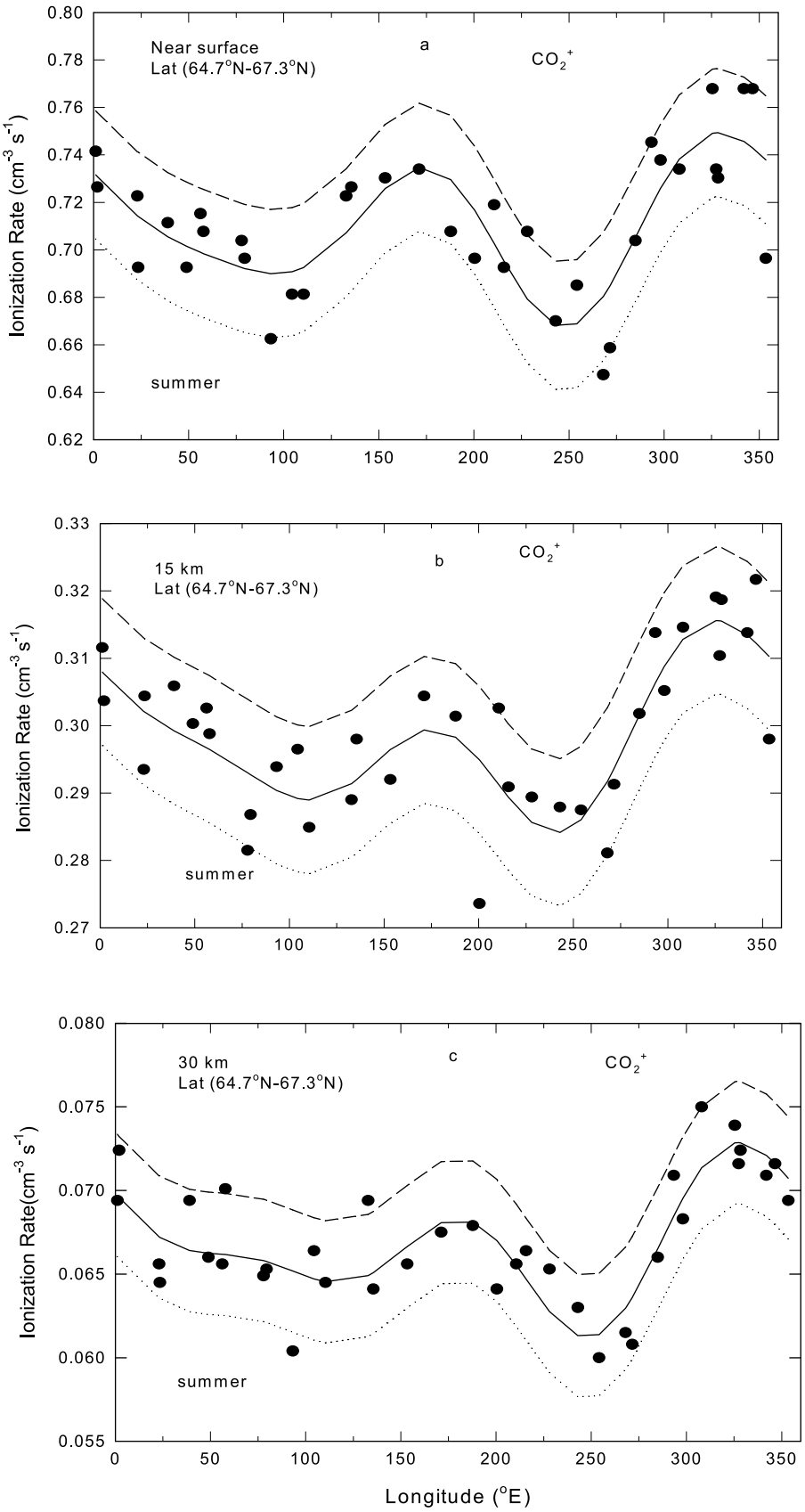

Figure 7. Model calculation of zonal structures of ionization rates of CO_2^+ during summer between longitudes 0° and 360°E and latitudes 64.7°N and 67.3°N at altitudes (a) near the surface, (b) 15 km, and (c) 30 km. The solid line represents the best fit to the calculation. The dotted and dashed lines represent lower and upper 0.95 confidence limits.

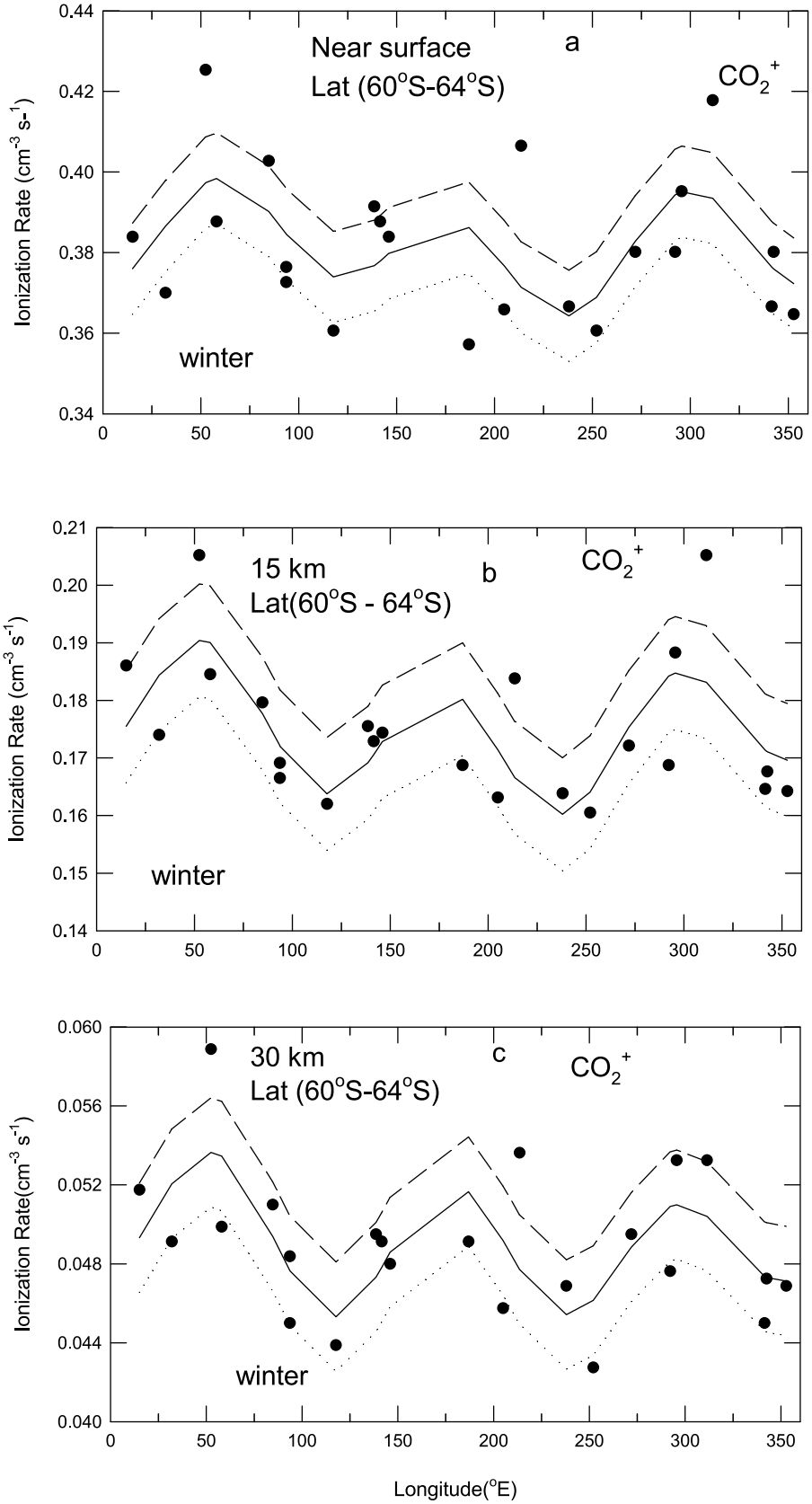

Figure 8. Model calculation of zonal structures of ionization rates of CO_2^+ during winter between longitudes 0° and 360°E and latitudes 60°S and 64°S at altitudes (a) near the surface, (b) 15 km, and (c) 30 km. The solid line represents the best fit to the calculation. The dotted and dashed lines represent lower and upper 0.95 confidence limits.

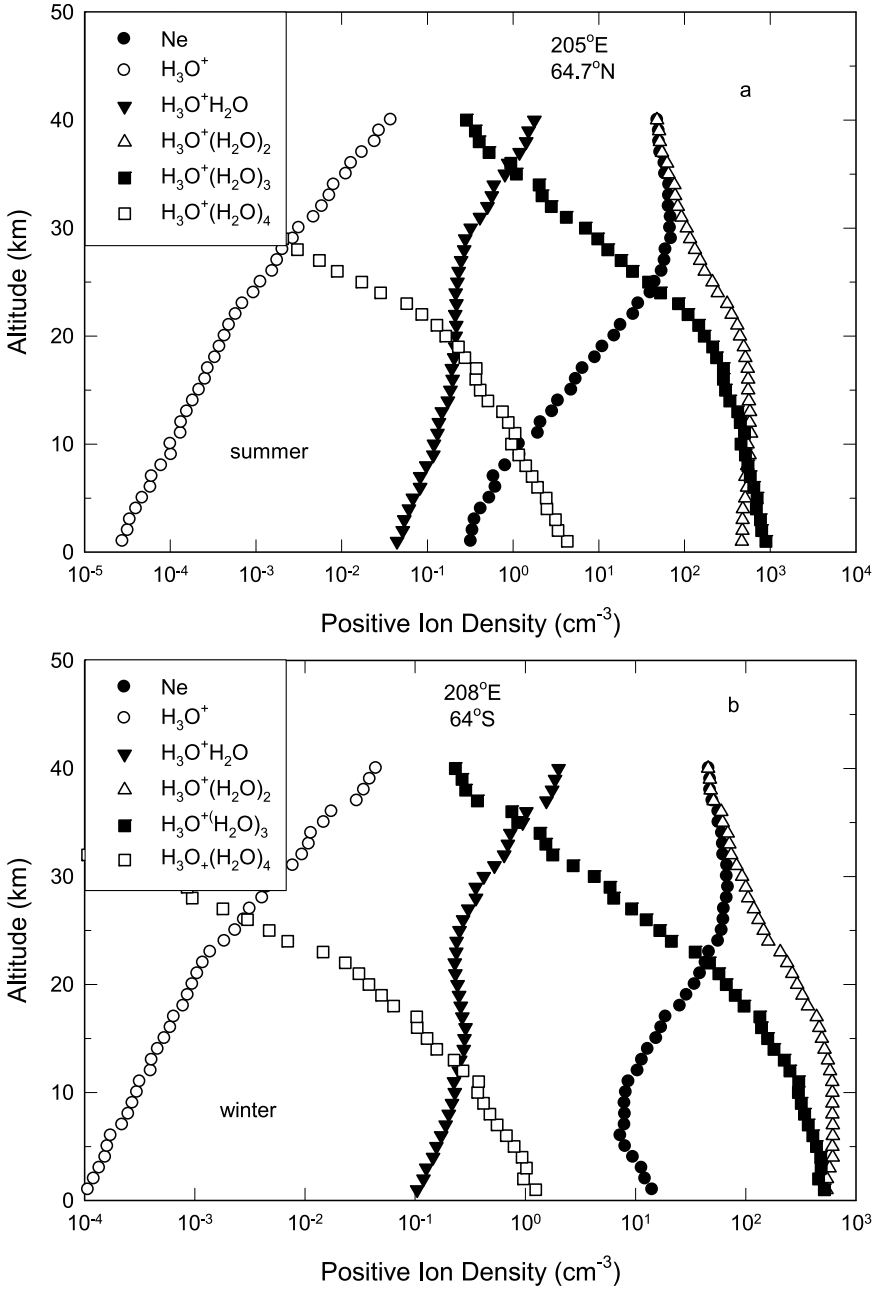

Figure 9. Altitude profiles of density of major positive ions and electron for (a) summer season at latitude 64.7° N and longitude 205°E and (b) winter season at latitude 64°S and longitude 208°E.

profiles of the *D* peak electron densities. However, there is a longitudinal delay of ~60° with the calculated values leading to the neutral density observations (Figures 3 and 4). This difference is associated with the value of λ, whose contribution is about ~10% in the peak electron density at ~30 km. With this value of λ, the positions of the crest and troughs in the peak electron density profiles will be shifted with respect to that obtained in the longitudinal distributions of neutral density and production rate. Therefore, the local maxima and minima in the calculated peak electron densities are being shifted from the neutral density data by ~60° eastward. This could be an important reason for the disappearance of the first peak at ~60°E in the peak electron density profile of the winter season (Figure 11b).

[19] In the troposphere of Mars, the ion neutral chemistry is similar to that of the *D* region of Earth's ionosphere, which is observed at altitude ~65–75 km mainly due to solar Lyman α radiation ionizing the minor constituent NO. The *D* region ionosphere of Earth does not present a clear peak electron density/or peak altitude but it refers to the height region below 95 km, which is not accounted for by the processes of the *E* region. Galactic cosmic rays, which affect the whole atmosphere down to the ground, become a major ionization source in the lower *D* region [cf. *Schunk and Nagy*, 2000]. X-rays do not contribute significantly to the *D* region ionosphere of Earth at sunspot minimum. At night the *D* layer on Earth begins to disappear because the primary source of ionization is no longer present and the

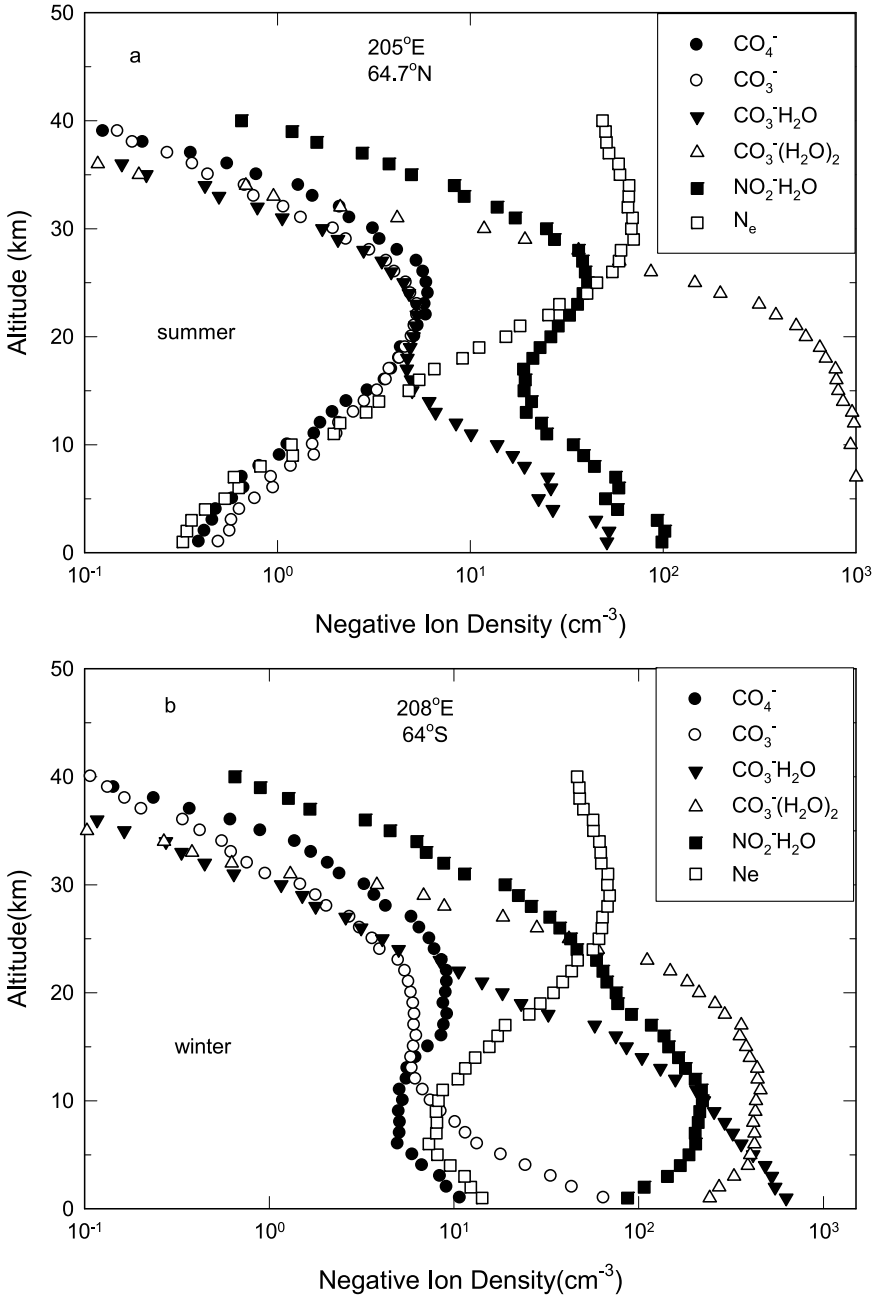

Figure 10. Altitude profiles of density of major negative ions and electron for (a) summer season at latitude 64.7°N and longitude 205°E and (b) winter season at latitude 64°S and longitude 208°E.

cosmic rays produce a residual amount of ionization. The ionization due to solar Lyman α is not considered in the lower ionosphere of Mars. This source will be almost ineffective because the density of NO is lower by 2–3 orders of magnitude in the Martian mesosphere as compared to that of the mesosphere of Earth [cf. *Aikin*, 1968; *Hargreaves*, 1992].The cosmic ray ionization has been found to be an important process for the formation of *D* layers in the daytime and nighttime ionosphere of Mars [*Whitten et al.*, 1971; *Molina-Cuberos et al.*, 2002; *Haider et al.*, 2007, 2009]. The column densities in the atmospheres of Mars and Earth are nearly $\sim 2.3 \times 10^{27}$ m^{-2} and $\sim 2.2 \times 10^{29}$ m^{-2}, respectively. Therefore cosmic rays penetrate deeper into the Martian atmosphere and form the *D* layer at lower altitudes than that observed in the Earth's ionosphere. The position and value of this peak layer are changing with longitude.

5. Future Direction

[20] In the dayside ionosphere, we have neither in situ measurements of low-altitude ion layers nor remote sensing measurements from the Mars surface. The direct measurements of cluster ions and electron density in the troposphere of Mars can be performed by Sounding rocket and Langmuir probe experiments on board future Mars missions. Sounding rockets carrying a quadrupole ion mass spectrometer have been found to be very useful experiments to

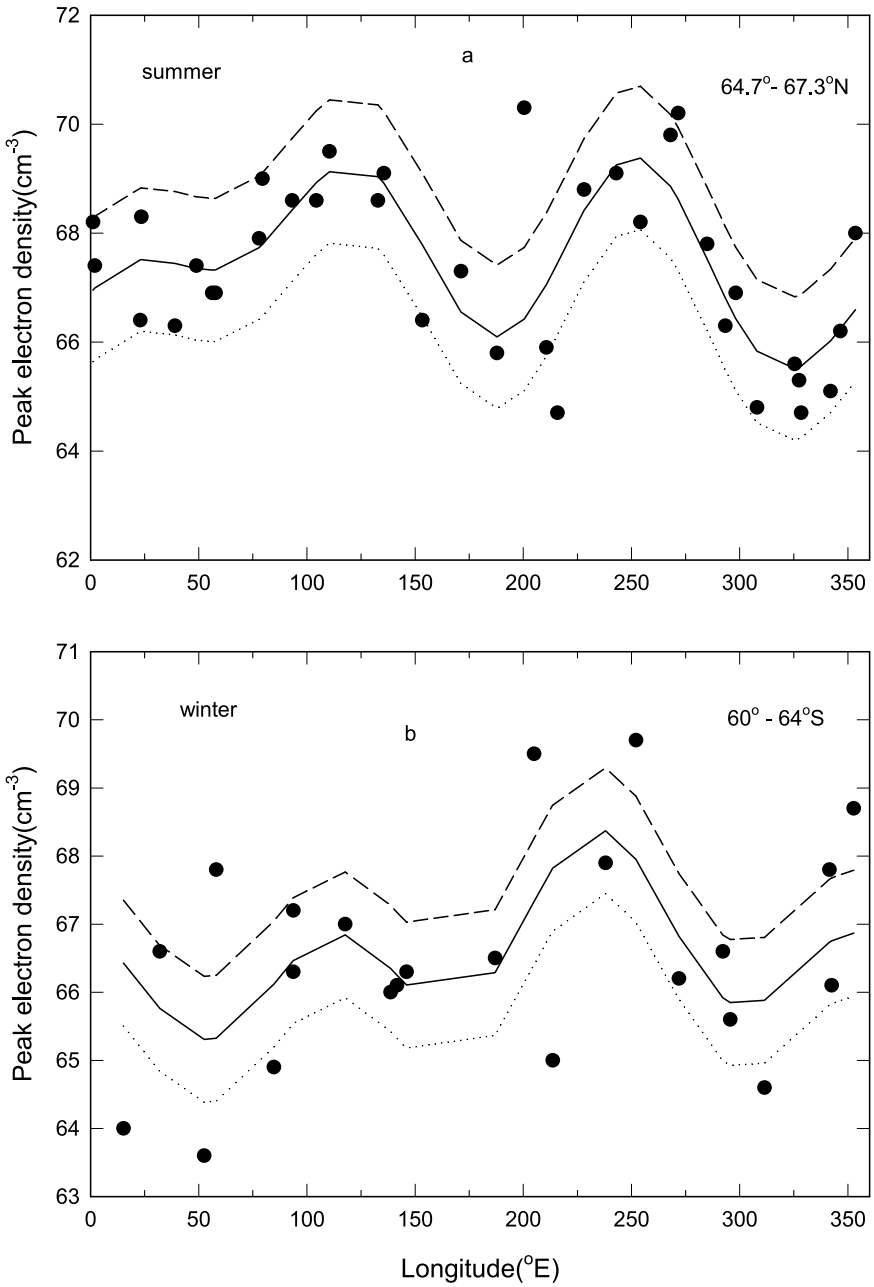

Figure 11. Longitudinal distribution of *D* peak electron densities for (a) summer season at latitude range 64.7°N–67.3°N and (b) winter season at latitude range 60°S–64°S in the nighttime ionosphere of Mars. The solid line represents the best fit to the calculation. The dotted and dashed lines represent lower and upper 0.95 confidence limits.

measure positive and negative ion densities in the *D* region of Earth's ionosphere. Langmuir probes have been used on rockets and balloons to measure electron density in the lower ionosphere of Earth. Ground-based remote sensing experiments such as very low frequency and incoherent scatter radars are used to measure the *D* layer on Earth. These two experiments can also be performed on Mars from a ground-based laboratory.

[21] The nighttime ionosphere of Mars has been observed from Mars 4 and Mars 5 spacecrafts [*Savich and Samovol*, 1976] by radio occultation experiments during the spring season. It appears that these measurements have observed a *D* layer shoulder of electron density between 500 cm^{-3} and 1500 cm^{-3} at altitude ~30–35 km. This signature is not very prominent and other published Mars low-altitude profiles do not show similar features [*Zhang et al.*, 1990]. These measurements have large error. The presence of plasma in these measurements is derived on the basis of a formal inversion of a set of observations using a symmetrical approximation. During the occultation measurements, the possible displacement of electron density due to this error was estimated to be ≈500 cm^{-3} [*Savich and Samovol*, 1976].

[22] It is generally accepted that global electric circuit over the Earth is driven by thunderstorm and lightning that are formed by charging of clouds. Clouds and dust particles have been observed in the troposphere of Mars as well [*Montmessin et al.*, 2006]. However, the electrical conductivity has not been observed in the Martian troposphere. Nevertheless charging would occur within the clouds observed on Mars. MarsNext and ExoMars are in the pipeline to explore conductivity on Mars by the European Space Agency. The objective of MarsNext is to study the global atmospheric system, meteorology and climate of Mars through a network of scientific stations on its surface [*Chicarro*, 2008]. With multiple stations, distributed across the surface of Mars, it will be possible to perform simultaneous measurements of the atmospheric winds, lightning and weather patterns in different seasons of Mars. This can be achieved by means of radio transmissions between the various Landers and a single orbiter. ExoMars will carry two instruments: (1) Atmospheric Relaxation and Electric Field Sensor (ARES) and (2) Martian Environmental Dust Systematic Analyser (MEDUSA). ARES is devoted to study the atmospheric electric field [*Hamelin et al.*, 2006]. It will measure the ionization state of the atmosphere, electric fields that results from the various charging mechanisms and will investigate the global electric circuit on Mars. MEDUSA will characterize the dust and water vapor environment close to the surface of Mars [*Esposito et al.*, 2008]. It will measure atmospheric dust particle size distribution, dust deposition rate and electrification (both positive and negative) of suspended dust particles in terms of charges per grain. We have calculated densities of positive ions, negative ions and electrons at different altitudes and longitudes in the troposphere of Mars. The water cluster ions $H_3O^+(H_2O)_{2,3}$ and $CO_3^-(H_2O)_{1,2}$ are the dominant species yielding a value of about $\sim 10^3$ cm^{-3} near the surface. The electrical conductivity produced by attachment of these ions to dust was found to be 4×10^{-12} ohm^{-1} m^{-1} close to the surface [*Michael et al.*, 2007]. This calculation can be useful to understand the global electric circuit system in the troposphere of Mars. In the absence of electric field and conductivity measurements in the troposphere over Mars, this calculation can be used as a diagnostic tool for future design of electrical payloads and for the subsequent data analysis to confirm the presence of lightning in the Martian troposphere.

6. Conclusion

[23] We have used MGS radio occultation data of temperature and air density to study zonal wave perturbations in the nighttime *D* region ionosphere of Mars during winter and summer seasons at latitudes 60°S–64°S and 64.7°N–67.3°N, respectively. These data are observed in the nighttime troposphere of Mars between longitudes 0° and 360°E at nearly the same solar longitude and same solar zenith angles. The data for the northern hemisphere were observed after midnight (at local time 0300–0400 h) on 24–31 December 1998 at Ls = 74°–77° and solar zenith angle 78°–81°. In the southern hemisphere the observations were performed in the late evening (after sunset at local time 2200–0100 h) on 2–15 March 1998 at Ls = 285°–291° and solar zenith angle 90°–93°. These data sets are used to calculate the production rate and densities of positive ions, negative ions and electrons in the summer and winter seasons of the two opposite hemispheres. We have found that the northern summer is dominated by wave number 2, while the southern winter is modulated by wave number 3 and 8. The modes 2 and 3 are due to the presence of thermal tides, which are planetary scale waves. These tides can propagate from the troposphere to the thermosphere by vertical transport coupling processes. These disturbances may be associated with the fixed topography of the Martian surface and therefore their associations to summer/winter conditions are arguable. The mode 8 is a rapidly moving transient disturbance, which may be associated with baroclinic instability process. The hydrated cluster ions ($H_3O^+(H_2O)_n$ for n = 1,2,3 and 4) and water cluster of NO_2^- and CO_3^- (i.e., $NO_2^-(H_2O)_n$ and $CO_3^-(H_2O)_n$ for n = 1,2) are dominated in the nighttime Martian troposphere. The maximum electron densities in winter and summer seasons are obtained at altitudes ~26 km and 30 km with the concentrations ~80 cm^{-3} and ~90 cm^{-3} at latitudes 64°S and 64.7°N, respectively because of the high efficiency of electron attachment to O_x molecules. The positive and negative ion densities are changed by factors of 5 to 10 between these two seasons due to the use of different model atmospheres. We have found strong effects of the zonal wave structure on the nighttime *D* region ionosphere of Mars during the winter and summer seasons at high southern and northern latitudes. Due to this effect, the peak electron densities are increased by 10% to 11% at longitudes 110°E and 240°E in the seasons of both hemispheres. The propagating mode number 2 of the semidiurnal tide is found to be the dominant cause of this enhancement in the *D* region ionosphere of Mars. It seems that the wave of high mode number 8 is weak and it is clustered with a strong wave number 2 in the *D* region ionosphere of Mars. Thus, the effect of baroclinic instability is limited to the air density and temperature of the troposphere only.

[24] **Acknowledgments.** The authors are thankful to the MGS science team at NASA's Planetary Data System for providing us data through the Web site http://pds-geosciences.wustl.edu/missions/mgs/radioscience.html. One of the authors, S. A. Haider, also thanks FAPESP for support through a visiting scientist fellowship by process 2007/06736-8 to work at INPE, Brazil.

[25] Amitava Bhattacharjee thanks the reviewers for their assistance in evaluating this paper.

References

Aikin, A. C. (1968), The lower ionosphere of Mars, *Icarus*, *9*, 487–497, doi:10.1016/0019-1035(68)90042-0.

Banfield, D., B. J. Conrath, M. D. Smith, P. R. Christensen, and R. J. Wilson (2003), Forced waves in the Martian atmosphere from MGS TES nadir data, *Icarus*, *161*, 319–345, doi:10.1016/S0019-1035(02)00044-1.

Barth, C. A., A. I. F. Stewart, S. W. Bougher, D. M. Hunten, S. J. Bauer, and A. F. Nagy (1992), Aeronomy of the current Martian atmosphere, in *Mars*, edited by H. Kiefer et al., pp. 1054–1089, Univ. of Ariz. Press, Tucson.

Bougher, S. W., S. Engel, D. P. Hinson, and J. M. Forbes (2001), Mars Global Surveyor radio science electron density profiles: Neutral atmosphere implications, *Geophys. Res. Lett.*, *28*, 3091–3094, doi:10.1029/2001GL012884.

Cavalie, T., F. Billeband, T. Enerenaz, M. Dobrijevic, J. Brillet, F. Forget, and E. Lellouch (2008), Vertical temperature profile and mesospheric winds retrieval on Mars from CO millimeter observations, *Astron. Astrophys.*, *489*, 795–809, doi:/10.1051/0004-6361:200809815.

Chicarro, A. F. (2008), MarsNext—A future major step in the European exploration of Mars, paper presented at 5th Meeting of AOGS, Asia Oceania Geosci. Soc., Busan, South Korea, 16–20 June.

Esposito, F., L. Colangeli, P. Palumbo, V. Della Corte, C. Molfese, J. Merrison, P. Nornberg, J. J. Lopez-Moreno, and J. Rodrigues Gomes (2008), Monitoring the airborne dust and water vapor in the low atmosphere of Mars: MEDUSA experiment for the ESA ExoMars mission, paper presented at 37th COSPAR Scientific Assembly, Comm. on Space Res., Montreal, Quebec, Canada, 13–20 July.

Haider, S. A., V. Singh, V. R. Choksi, W. C. Maguire, and M. I. Verigin (2007), Calculated densities of $H_3O^+(H_2O)_n$, $NO_2^-(H_2O)_n$, CO_3^- $(H_2O)_n$ and electron in the nighttime ionosphere of Mars: Impact of solar wind electron and galactic cosmic rays, *J. Geophys. Res.*, *112*, A12309, doi:10.1029/2007JA012530.

Haider, S. A., V. Sheel, V. Singh, W. C. Maguire, and G. J. Molina-Cuberos (2008), Model calculation of production rates, ion and electron densities in the evening troposphere of Mars at latitudes 67°N and 62°S: Seasonal variability, *J. Geophys. Res.*, *113*, A08320, doi:10.1029/2007JA012980.

Haider, S. A., M. A. Abdu, I. S. Batista, J. H. Sobral, X. Luan, E. Kallio, W. C. Maguire, M. I. Verigin, and V. Singh (2009), *D*, *E*, and *F* layers in the daytime at high-latitude terminator ionosphere of Mars: Comparison with Earth's ionosphere using COSMIC data, *J. Geophys. Res.*, *114*, A03311, doi:10.1029/2008JA013709.

Hamelin, M., K. Szegö, M. Godefroy, J. J. Berthelier, F. Simões, and the ARES team (2006), ARES: An atmospheric electricity instrument proposed for EXOMARS. Results of balloon tests in the terrestrial atmosphere, paper presented at European Planetary Science Congress 2006, Eur. Planetol. Network, Berlin, 18–22 Sept.

Hargreaves, J. K. (1992), *The Solar Terrestrial Environment: An Introduction to Geospace—Science of the Terrestrial Upper Atmosphere, Ionosphere and Magnetosphere*, Cambridge Univ. Press, Cambridge, U. K.

Hinson, D. P., R. A. Simpson, J. D. Twicken, G. L. Tyler, and M. Flassar (1999), Initial results from radio occultation measurements with Mars Global Surveyor, *J. Geophys. Res.*, *104*, 26,997–27,012, doi:10.1029/1999JE001069.

Hollingsworth, J. L., and J. R. Barnes (1996), Forced stationary planetary waves in Mars' winter atmosphere, *J. Atmos. Sci.*, *53*, 428–448, doi:10.1175/1520-0469(1996)053<0428:FSPWIM>2.0.CO;2.

Imamura, T., and T. Ogawa (1995), Radiative damping of gravity waves in the terrestrial planetary atmospheres, *Geophys. Res. Lett.*, *22*, 267–270, doi:10.1029/94GL02998.

Mahajan, K. K., and J. Kar (1988), Planetary ionospheres, *Space Sci. Rev.*, *47*, 303–397, doi:10.1007/BF00243558.

Mahajan, K. K., S. Singh, A. Kumar, S. Raghuvanshi, and S. A. Haider (2007), Mars Global Surveyor radio science electron density profiles: Some anomalous features in the Martian ionosphere, *J. Geophys. Res.*, *112*, E10006, doi:10.1029/2006JE002876.

Martin, L. J. (1984), Clearing the Martian air: The troubled history of dust storms, *Icarus*, *57*, 317–321, doi:10.1016/0019-1035(84)90120-9.

Michael, M., M. Barani, and S. N. Tripathi (2007), Numerical predictions of aerosol charging and electrical conductivity of the lower atmosphere of Mars, *Geophys. Res. Lett.*, *34*, L04201, doi:10.1029/2006GL028434.

Molina-Cuberos, G. J., H. Lichtenegger, K. Schwingenschuh, J. J. López-Moreno, and R. Rodrigo (2002), Ion-neutral chemistry model of the lower ionosphere of Mars, *J. Geophys. Res.*, *107*(E5), 5027, doi:10.1029/2000JE001447.

Montmessin, F., E. Quémerais, J. L. Bertaux, O. Korablev, P. Rannou, and S. Lebonnois (2006), Stellar occultations at UV wavelengths by the SPICAM instrument: Retrieval and analysis of Martian haze profiles, *J. Geophys. Res.*, *111*, E09S09, doi:10.1029/2005JE002662.

Nair, H., M. Allen, A. D. Anbar, Y. L. Yung, and R. T. Clancy (1994), A photochemical model of the Martian atmosphere, *Icarus*, *111*, 124–150, doi:10.1006/icar.1994.1137.

Rodrigo, R., E. García-Álvarez, M. J. López-González, and J. J. López-Moreno (1990), A nonsteady one-dimensional theoretical model of Mars' neutral atmospheric composition between 30 and 200 km, *J. Geophys. Res.*, *95*, 14,795–14,810.

Savich, N. A., and V. A. Samovol (1976), The night time ionosphere of Mars from Mars 4 and Mars 5 dual-frequency radio occultation measurements, *Space Res.*, *XVI*, 1009–1011.

Schunk, R. W., and A. F. Nagy (2000), *Ionospheres: Physics, Plasma Physics, and Chemistry*, Cambridge Univ. Press, Cambridge, U. K.

Seth, S. P., and V. Brahmananda Rao (2008), Evidence of baroclinic waves in the upper atmosphere of Mars using the Mars Global Surveyor accelerometer data, *J. Geophys. Res.*, *113*, A10305, doi:10.1029/2008JA013165.

Seth, S. P., V. Brahmananda Rao, C. M. Esprito Santo, S. A. Haider, and V. R. Choksi (2006), Zonal variations of peak ionization rates in upper atmosphere of Mars at high latitude using Mars Global Surveyor accelerometer data, *J. Geophys. Res.*, *111*, A09308, doi:10.1029/2006JA011753.

Tyler, G. L., G. Balmino, D. P. Hinson, W. S. Sjogren, D. E. Smith, R. A. Simpson, S. W. Asmar, P. Priest, and J. D. Twicken (2001), Radio science observations with Mars Global Surveyor: Orbit insertion through one Mars year in mapping orbit, *J. Geophys. Res.*, *106*, 23,327–23,348, doi:10.1029/2000JE001348.

Whittaker, E., and G. Robinson (1967), *The Calculus of Observations; An Introduction to Numerical Analysis*, 397 pp., Dover, Mineola, N. Y.

Whitten, R. C., I. G. Poppoff, and J. S. Sims (1971), The ionosphere of Mars below 80 km altitude—I. Quiescent conditions, *Planet. Space Sci.*, *19*, 243–250, doi:10.1016/0032-0633(71)90203-0.

Zhang, M. H. G., J. G. Luhmann, and A. J. Kliore (1990), An observational study of the nightside ionosphere of Mars and Venus with radio occultation methods, *J. Geophys. Res.*, *95*, 17,095–17,107, doi:10.1029/JA095iA10p17095.

M. A. Abdu, I. S. Batista, and J. H. A. Sobral, Instituto Nacional de Pesquisas Espaciais, Ave. dos Astronautas 1758, Jd. Granja, São José dos Campos, São Paulo 12201-970, Brazil.

S. A. Haider and V. Sheel, Physical Research Laboratory, Navrangpura, Ahmedabad 380 009, India. (haider@prl.res.in)

W. C. Maguire, NASA Goddard Space Flight Center, Mail Code 693, Greenbelt, MD 20771, USA.

G. J. Molina-Cuberos, Universidad de Murcia, PO Box 4021, E-30100 Murcia, Spain.

M. I. Verigin, Space Research Institute, Profsoyuznaya 84/32, Moscow 117997, Russia.